Detection, Measurement and Characterization of Inclusions Using Automated SEM Techniques Part 1: The Effects of Pixel Spacing, X-Ray Collection Time and Accelerating Voltage

Henry P. Lentz, Michael S. Potter, Gary S. Casuccio

RJ Lee Group, Inc.
350 Hochberg Road, Monroeville, PA, USA, 15146
Phone: 724-325-1776
Email: hlentz@rjleegroup.com

Keywords: Inclusions, SEM, automated electron microscopy, steel cleanliness, CCSEM

INTRODUCTION

Scientists and engineers have long studied the microscopic properties of steel in order to predict macroscopic properties of both the steel and the steel-making process. As early as the 1920s, steel cleanliness was evaluated using light-optical microscopes with a procedure that later became well known as the JK (Jernkontoret) rating system[1]. With the advent of Transmission Electron Microscopes (TEMs) and X-ray analysis systems, steel could be analyzed at higher magnifications and the morphology and composition of structures could be more easily and accurately quantified. Figure 1(a) shows Dr. Robert Fisher operating a system combining "a modified [transmission] electron microscope with an X-ray analyzer to establish the composition of microscopic particles in steel" at U. S. Steel's Research Center in 1956.[2]

(a) (b)

Figure 1 – (a) Electron Microscope Inclusion Analysis System at U. S. Steel Research Center, 1956; (b) Early CCSEM System at U. S. Steel Research Center, Monroeville, PA, Circa 1979

In the 1960s, Scanning Electron Microscopes (SEMs) became commercially available, and with the SEM it became possible to routinely perform "surface analysis" without the limitations of sample-size and thickness imposed by the TEM.

As digital technology became more compact, inexpensive, and accessible in the 1970s, computer control began to be applied to both optical and electron microscopes in order to automate the analysis process. This improved the analysis process in several ways – faster analysis, data that is more repeatable and bias-free, and reduction of operator error and fatigue. Figure 1(b) shows an early Computer-Controlled Scanning Electron Microscope (CCSEM) system at the U. S. Steel Research Center, circa 1979, with Dr. Richard Lee at the SEM console, surrounded by minicomputer-based beam control and X-ray analysis systems.[3]

Optical microscopy benefits from motorized stage mechanisms and image analysis, while the application of computer control to an SEM adds automation of optics, beam positioning, and both electron- and X-ray detectors, as well as spectral analysis.

CCSEM for analyzing particles (such as inclusions) involves several core processes: (1) Particle detection, (2) Size/shape measurement, and (3) Determination of composition. These core processes are then wrapped in a workflow that permits the analysis of multiple fields of view, multiple samples, and database storage of images, spectra, and other numeric data.

One of the great benefits of the SEM is the backscattered electron (BSE) mechanism of image formation. Image contrast in BSE mode is a function of the atomic number of the material – heavier elements appear brighter in a BSE image. Brightness of compounds or mixtures is the weighted average of the mass of the constituent elements[4]. Therefore, it is straightforward to use image-analysis techniques to detect and measure inclusion particles in the higher-atomic-number metal. A second benefit is that the beam/specimen interaction generates X-rays, the energies of which are highly characteristic of the elements in the particle. By accumulating the energies of the X-ray photons in a histogram-type of structure, a spectrum is created with peaks indicating the presence and relative quantities of the elements at the beam location on the sample. With these attributes, CCSEM technology has been investigated as an inclusion analysis tool for several decades.[5] Today, CCSEM analysis of inclusions is evolving into a standard practice in the steel industry[6,7,8] and indeed has been incorporated into standard methods for inclusion analysis[9].

However, one of the challenges of CCSEM inclusion analysis is the fact that inclusions are generally sparse relative to the total surface area of a sample – typically 1% or much less. Therefore, much of the effort in creating efficient CCSEM software – such as the Automated Steel Cleanliness Analysis Tool[10] (ASCAT) used in this study (shown in Figure 2) is to maximize the time spent on areas of interest – the inclusions – and minimize the time spent on the bare steel where there is no useful information to acquire. ASCAT uses a dual-mode imaging approach to accomplish this. The steel is scanned using a fairly low magnification, where the pixel spacing is just close enough to ensure that at least one pixel intersects the smallest inclusion to be analyzed. Then, the software zooms up to a higher magnification, but just in the vicinity of the inclusion, and collects a *microimage*[11] with many pixels on the particle to allow accurate measurement. This has the added benefit that the microimage of each inclusion can be saved for post-analysis review.

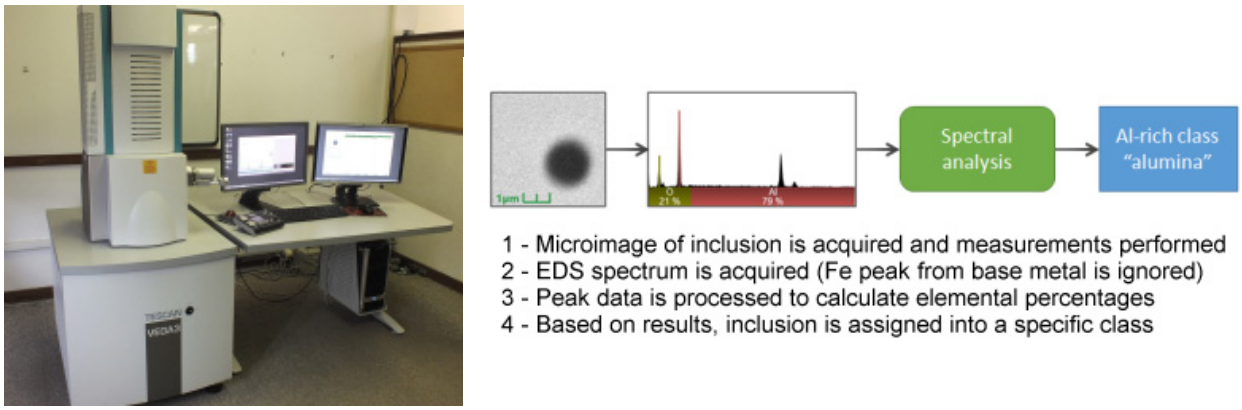

Figure 2 - Photo of ASCAT System and Schematic of Process of Inclusion Analysis and Identification.

Since X-ray signals are much sparser than electron signals, the beam is placed directly on each inclusion for collecting an X-ray spectrum, so that time is not wasted collecting X-ray data on areas of low information content.

This paper is the first of a series that will provide insight on the application of CCSEM techniques to characterize inclusions. In this paper, we discuss some of the implications and the speed-versus-accuracy/precision tradeoffs of different parameters

and settings on ASCAT analysis, with experiments performed on a TESCAN Vega3 SEM, Bruker Quantax Energy Dispersive Spectrometer, and ASCAT software, which is based on RJ Lee Group's IntelliSEM™ CCSEM software platform:

- Search-Pixel Spacing – trade off the speed of the inclusion-search phase versus statistical uncertainty in the small-inclusion population.
- X-ray Collection Time – trade off speed versus quantification certainty
- Accelerating Voltage – trade off beam-penetration versus signal generation and image resolution

BACKGROUND – CCSEM PROCESS FOR INCLUSION ANALYSIS

The Scanning Electron Microscope/Energy Dispersive Spectrometer (SEM/EDS) is a powerful and versatile tool for materials analysis, and can be used in a variety of ways for the analysis of inclusions in metal in general, and steel cleanliness in particular. Much can be learned through detailed manual analysis of individual inclusions, and manual analysis is an important approach to understanding the nature of inclusions found in steel. Manual analysis, however does not lend itself to efficient statistical analysis of inclusion populations. For such studies, manual analysis is a labor-intensive endeavor – time consuming, error-prone, and fatigue inducing for even modest particle populations.

The ASCAT is designed to permit automated collection of size, shape, and chemical information for vast particle populations with little or no human intervention. While it is possible to use ASCAT for quasi-manual data collection, i.e., high-spatial-resolution imagery and extended chemical analysis on each inclusion, the technique is really designed for a different challenge – acquire sufficient statistical information to answer the question in the shortest possible time. Especially in a production environment, where "time is money," it is critical to provide adequate information while minimizing sample turnaround time.

The general process of ASCAT can be thought of as a series of nested loops. Innermost is the analysis of a single particle; this is repeated for each particle in a field-of-view; this in turn is repeated for all fields-of-view on a sample. Analyzing multiple samples represents the outermost loop. Modern SEM/EDS systems allow stage movement, beam positioning, and image/signal acquisition to be performed entirely under software control.

Inclusions generally represent a minute percentage of the surface of a steel sample, which presents both challenge and opportunity for CCSEM analysis. The challenge is that a large area needs to be searched, most of which contains no inclusions and therefore no useful information. The opportunity is that CCSEM software can manage its process in such a way that information-sparse sample areas are scanned very rapidly, while spending more time analyzing information-dense areas (inclusions). In this way, valuable time is spent where it is most beneficial.

As stated earlier, there are three main activities performed by CCSEM: (1) Search/Detect; (2) Measure inclusion size/shape; (3) Perform chemical analysis on inclusion.

The Search/Detect process involves finding inclusions within each field-of-view. The fields, using modern digital technology, are a rectangular grid of pixels, and as such can be processed using image analysis techniques, or by filtering the pixels as they are acquired. In either case, the backscattered electron (BSE) signal, as discussed in the previous section, provides atomic-number contrast between the steel matrix and the non-metallic (and other) inclusions, such that the computer can discriminate the location of inclusions.

Once inclusions are located, their size and shape can be measured using the same BSE signal. The dichotomy here is that, in order to make accurate and repeatable measurements, a relatively dense pixel spacing is required – essentially the pixel spacing is analogous to the divisions on a ruler; the more divisions, the more precise the measurement can be. On the other hand, the denser the pixel spacing, the longer it will take to search for inclusions in the first place.

For this reason, CCSEM systems typically use a dual pixel-density approach to search and sizing. Wider spacing is used while searching for inclusions, while tighter spacing is used for measurement. Some systems use a live-beam, rotated-chord approach, shown in Figure 3(a) while others, such as the ASCAT that was used for this study, use a microimage approach as shown in Figure 3(b). The microimage approach, in which a zoomed image is acquired at the location of each inclusion, has the advantage of automatically generating a digital image of each inclusion that can be stored with the rest of the data, and in the absence of gross instrument drift provides reliable measurement of the detected inclusions.

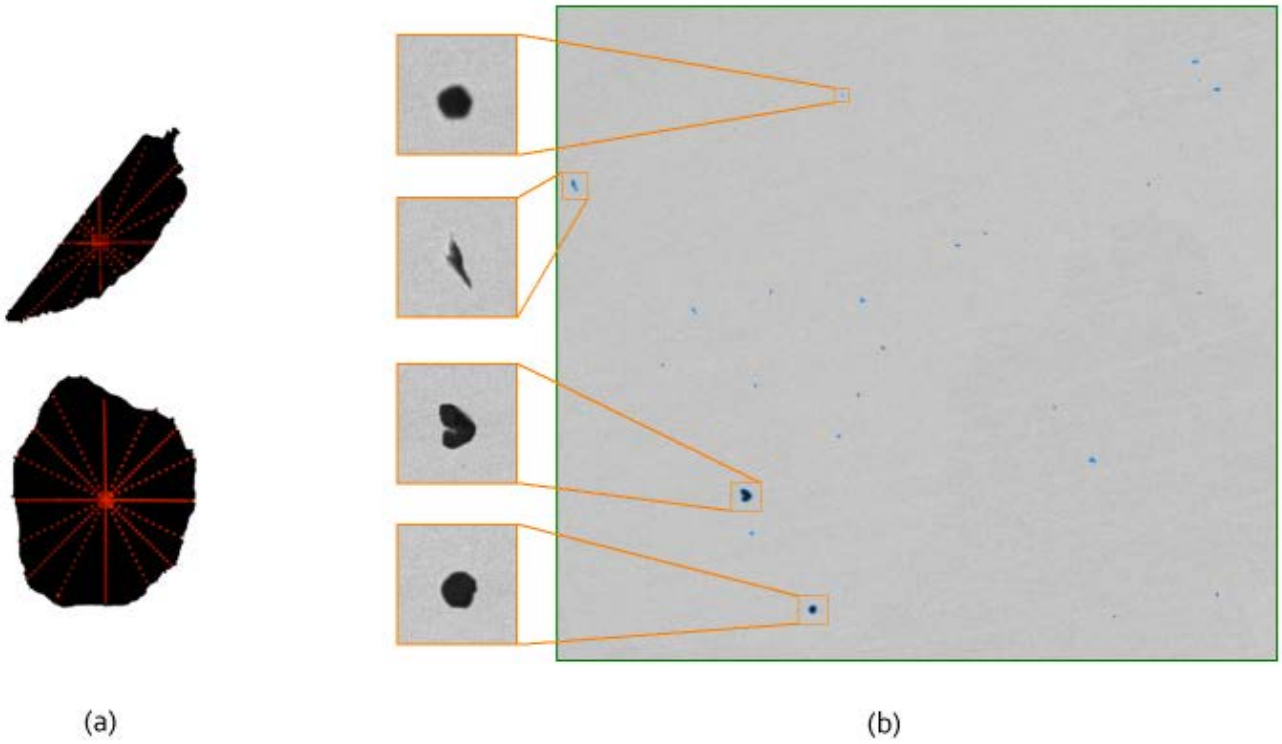

Figure 3 - (a) Rotated-chord measurement technique; (b) Microimage measurement technique

The tradeoffs involved in selection of pixel spacing during the search phase are discussed further in the next section.

Once the inclusion has been detected and measured, the next step is to determine the elemental composition of the inclusion. This is typically done using EDS which detects X-ray photons that are generated by the interaction of the electron beam with the sample. While the BSE signal is proportional to the average atomic number of the material, the EDS signal is much more highly selective of the actual elemental constituents. For this reason, EDS is used for performing elemental/chemical analysis.

This raises the question, 'why not use EDS for search as well?" While technically it is possible to use EDS for search, it is much less efficient than using BSE for this reason: While approximately 5-50% of incident electrons will yield backscatter electrons[12], the probability of X-ray generation is several orders of magnitude lower and would require significantly more time per pixel.

With the beam on the inclusion, X-rays are collected for a sufficient time to allow identification of the inclusion species, as discussed in a subsequent section.

The following sections discuss some of the tradeoffs that should be considered when determining analysis conditions when performing CCSEM analysis on inclusions in steel.

SEARCH-PIXEL SPACING

Search, whether using live-beam or stored-image techniques, involves detecting inclusions within a field-of-view using backscattered electron (BSE) contrast. Consider the second inclusion in Figure 3(b). Once this inclusion is detected in the field-of-view using image analysis techniques, the CCSEM software automatically zooms and pans the acquisition area in order to acquire a higher-resolution image in the area of the inclusion; similar image processing techniques can then be used to measure the inclusion with improved accuracy. Figure 4(a) shows the appearance of the inclusion in the field image – the pixilation is due to the relatively wide pixel spacing – and Figure 4(b) shows its appearance in the zoomed microimage. This illustrates the benefit of widely-space pixels – while the inclusion cannot be measured accurately in the field image it can easily be detected, while minimizing the amount of time required to scan the steel matrix. Since halving the pixel spacing increases the number of pixels – and therefore search time – by a factor of four, there is a great speed benefit gained by keeping search spacing as wide as possible while only using close pixel spacing in the immediate vicinity of inclusions.

While the inclusion in Figure 4(a) and 4(b) is represented by multiple pixels in the field image, it is really only necessary to have one field-image pixel within threshold in order to register and trigger a microimage acquisition. Figure 4(c) illustrates

that a single pixel in the field of view allows the CCSEM software to detect the inclusion, and then zoom up to make a more accurate size measurement as shown in Figure 4(d).

While it might seem that pixel spacing equal to minimum inclusion size is required to ensure detection, it is actually a more complex function of inclusion size and shape, beam characteristics, interaction volume, and inclusion/matrix constituents. However, for simplicity, consider the case of a spherical inclusion with an infinitesimally small beam diameter and excitation volume. Figure 4(e) shows inclusions of various sizes superimposed upon a search grid of pixels. There is a certain inclusion size at or above which detection probability is 1.0 (100%). For this simplified case, if the pixel spacing is D_p, a "unity probability diameter" D_{unity} can be defined as $D_p\sqrt{2}$, in other words, the diameter of the inclusion must equal the diagonal spacing across a single pixel grid. Thus, in order to ensure unity probability of detection, the inclusion diameter must be approximately 1.414 times the horizontal/vertical pixel spacing. As noted previously, this neglects such effects as finite beam diameter and non-uniform spatial density of the beam, as well as inclusion geometry and excitation depth/spread. Therefore, the true value of D_{unity} may be more or less than that indicated by our simplified model. However, for the purposes of this discussion, we can assume that these effects will be held constant for different pixel spacing.

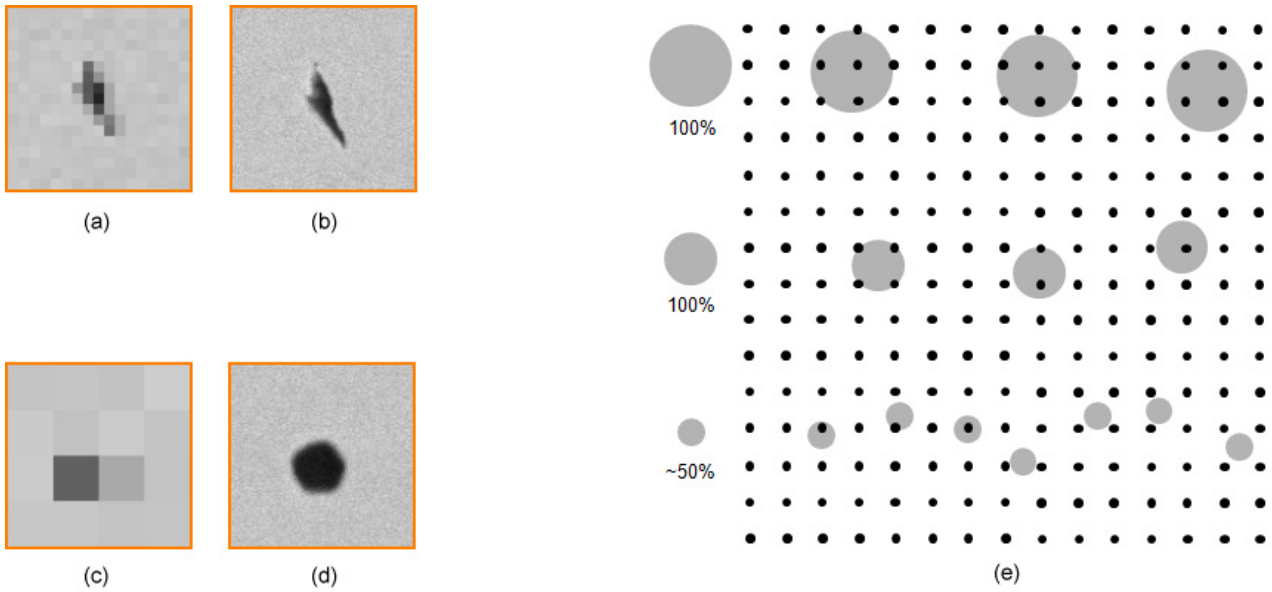

Figure 4 – Detection of Inclusions in CCSEM Search Mode: (a) Multi-Pixel Inclusion in Search Field; (b) Same Inclusion in Microimage; (c) Single-Pixel Inclusion in Search Field; (d) Same Inclusion in Microimage; (e) Simplified Schematic of Detection Probability

There is potential to decrease analysis time by performing CCSEM analysis by way of *spatial undersampling* – in other words, pixel spacing greater than D_{unity}. In this case, one is accepting that a certain percentage of smaller inclusions will be missed in order to greatly reduce the time required to search a large area for inclusions. When undersampling, the detection probability as a function of inclusion size can be used to compute a scaling factor associated with each inclusion that is found. Again, using the simplified model discussed above, the detection probability for an inclusion of diameter D_i can be expressed as follows (Equation 1 and 2):

$$P(D_i) = (D_i / D_{unity})^2 \qquad \text{for } D_i < D_{unity} \tag{1}$$

$$P(D_i) = 1.0 \qquad \text{for } D_i \geq D_{unity} \tag{2}$$

On this basis, Equation 3 shows a scaling factor can be derived as the multiplicative inverse of the probability:

$$S(D_i) = 1.0/P(D_i) \tag{3}$$

Essentially, this is a "missed inclusion" scaling factor. It accounts for the fact that, due to spatial undersampling, a certain percentage of inclusions of this description will be found, and a certain percentage will be missed.

Example: Suppose an inclusion is found with diameter $D_{unity}/2.0$. In this case, the detection probability $P(D_i)$ will equal 0.25, and therefore the scaling factor is 4.0. In other words, such an inclusion has a 25% probability of being detected, so for each inclusion like this which is found, three can be assumed to be missed due to spatial undersampling. Therefore, when constructing distributions and summarizing data, we can treat this inclusion as if it is four identical inclusions (the one that was found plus the three that were missed).

Figure 5 provides histograms of the area fraction from two samples that were analyzed with the ASCAT using pixel spacing varying from 0.5 µm to 3.0 µm. The lower bound on the particle size was set to 1.0 µm so no scaling factor would be applied to the 0.5 and 1.0 µm pixel-spacing analyses. Figure 5(a) and 5(c) represent the raw measured values (in area percent) for each analysis. For Sample A349, similar results were obtained using pixel-spacing values of 0.5, 1.0 and 2.0 µm. However, 3.0 µm pixel spacing resulted in a decrease of about 25 percent as compared to the 'true' value. For Sample A364, a decrease in area fraction of ~40 percent and ~55 percent was observed using a pixel spacing values of 2.0 µm and 3.0 µm. However, by scaling the data using the probability model discussed above, the area fraction results for all pixel-spacing values were similar, as illustrated in Figures 5(b) and 5(d). These data show that spatial undersampling with probability-based scaling can provide a reasonably accurate estimate of the small-inclusion population.

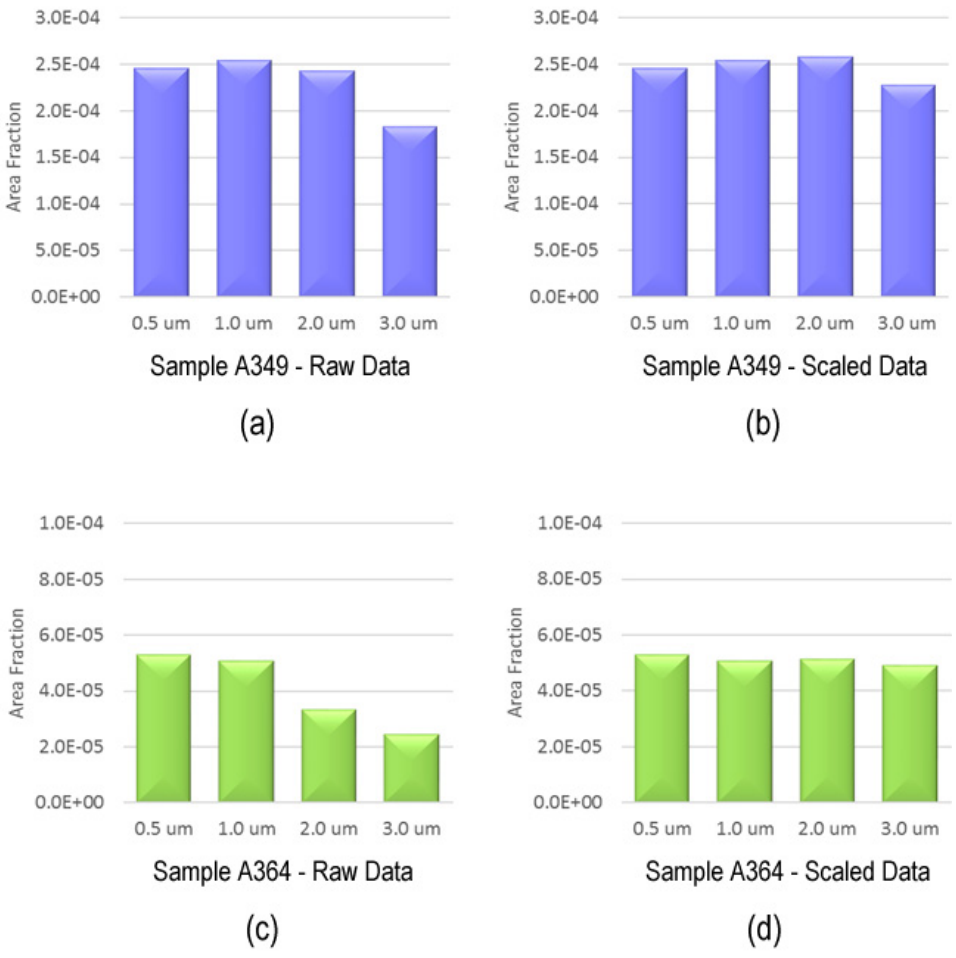

Figure 5. Area Fraction of Inclusions Using Different Pixel Densities.

The real payoff is the improvement in analysis speed that is possible with spatial undersampling. Table 1 shows the analysis time (normalized to a 100mm^2 area) for analyses performed for Figure 5.

Table I - Normalized Analysis Time (minutes) per 100 mm^2 Using Various Pixel Spacing

Sample	Pixel Spacing (µm)			
	0.5	**1.0**	**2.0**	**3.0**
A349	365	135	53	20
A364	170	80	43	20

Some general statements can be made when evaluating the tradeoffs associated with selection of pixel spacing and evaluation of undersampling for a particular application:

- For large sample areas, a significant improvement in speed is possible by spatial undersampling
  - Doubling pixel spacing reduces search time by a factor of 4.
  - Tripling pixel spacing reduces search time by a factor of 9.
- For "dirty" samples (many inclusions), X-ray acquisition may be the dominant contributor to total analysis time; for such samples, search-speed improvement may not be as significant.
- Statistical scaling produces a reasonable estimate of small-inclusion population.
  - Small-inclusion population must be sufficient to allow valid statistics.

CONSIDER undersampling if:

- Analysis speed is critical.
- Estimating small-inclusion population does not prevent ASCAT data from providing reliable answers for the application.

AVOID undersampling if:

- Highly accurate characterization and/or number-distribution is required on smallest inclusions.
- Small-inclusion population includes rare-phase(s) which may not be abundant enough for valid scaling statistics.

X-RAY COLLECTION TIME

ASCAT acquires an EDS spectrum for each inclusion analyzed. Because the BSE signal generated by the beam is much stronger than the X-ray signal, the collection time when acquiring X-ray spectrum is generally on the order of 1 second, while the pixel-dwell time in BSE mode while searching for inclusions is more on the order of 1µs. So certainly any time saved performing an EDS analysis can have a significant effect on overall analysis time depending on the number of inclusions on the sample area.

The purpose of acquiring an X-ray spectrum is to determine the chemical/elemental composition of the inclusion, and this can be done in a variety of ways, from as simple as computing normalized count percentages based on the background-subtracted area under the peaks, to as complex as a standards-based quantitative analysis that accounts for beam dose and characteristics, sample/detector geometry, and the effects of fluorescence/absorption/atomic-number of the constituent elements.

We now may ask:

- What constitutes appropriate analytical information to answer the questions posed for a particular application?
- How much EDS data is required to generate that information?

Consider Figure 6, which shows an EDS acquisition from a single inclusion using different acquisition times. In this case, the instrument conditions were set up for a count rate of 45 thousand counts per second (kcps) for each spectrum. With just a quick glance, it appears that the spectra are nearly identical, with the exception of more noise, or "hash" in the spectra acquired with shorter collection times.

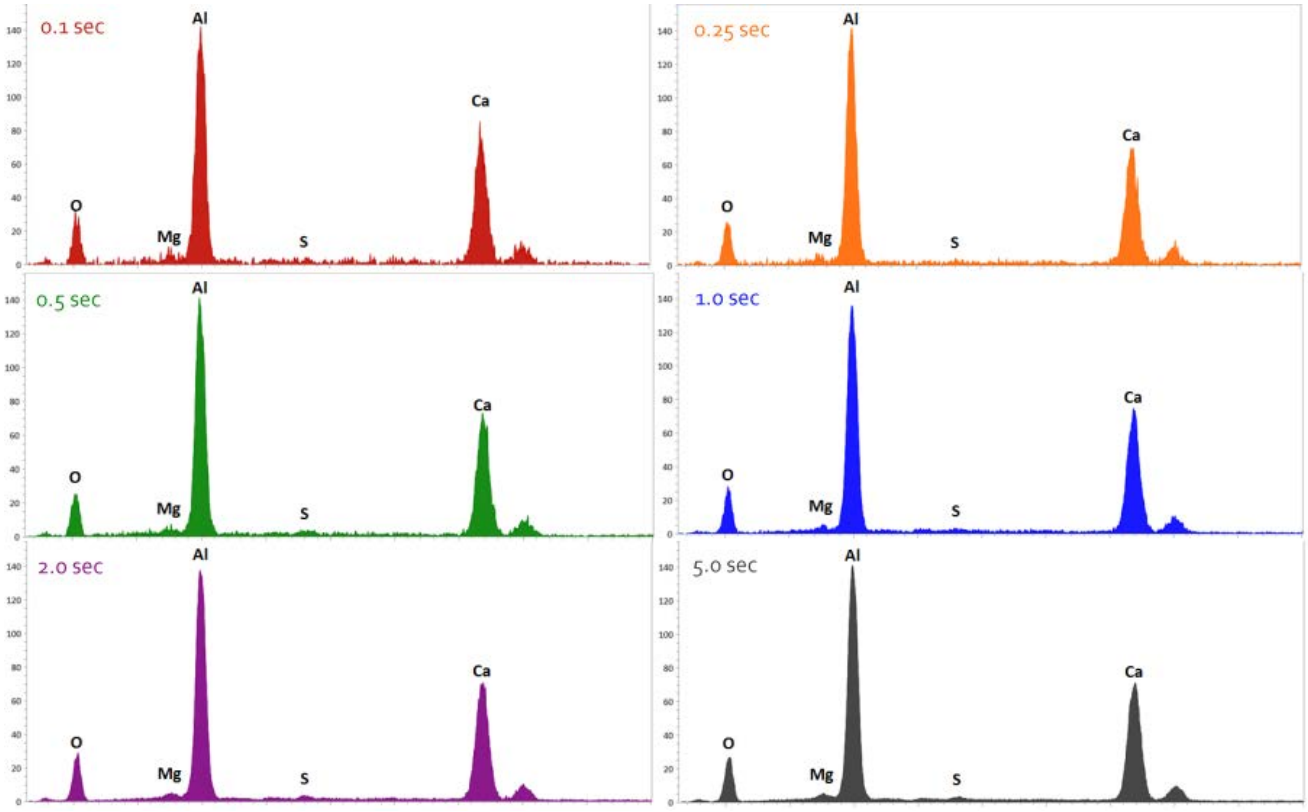

Figure 6 - - EDS Spectra at 45Kcps of Single Spectra at Various Collection Times. Horizontal Scale is 0-5 keV

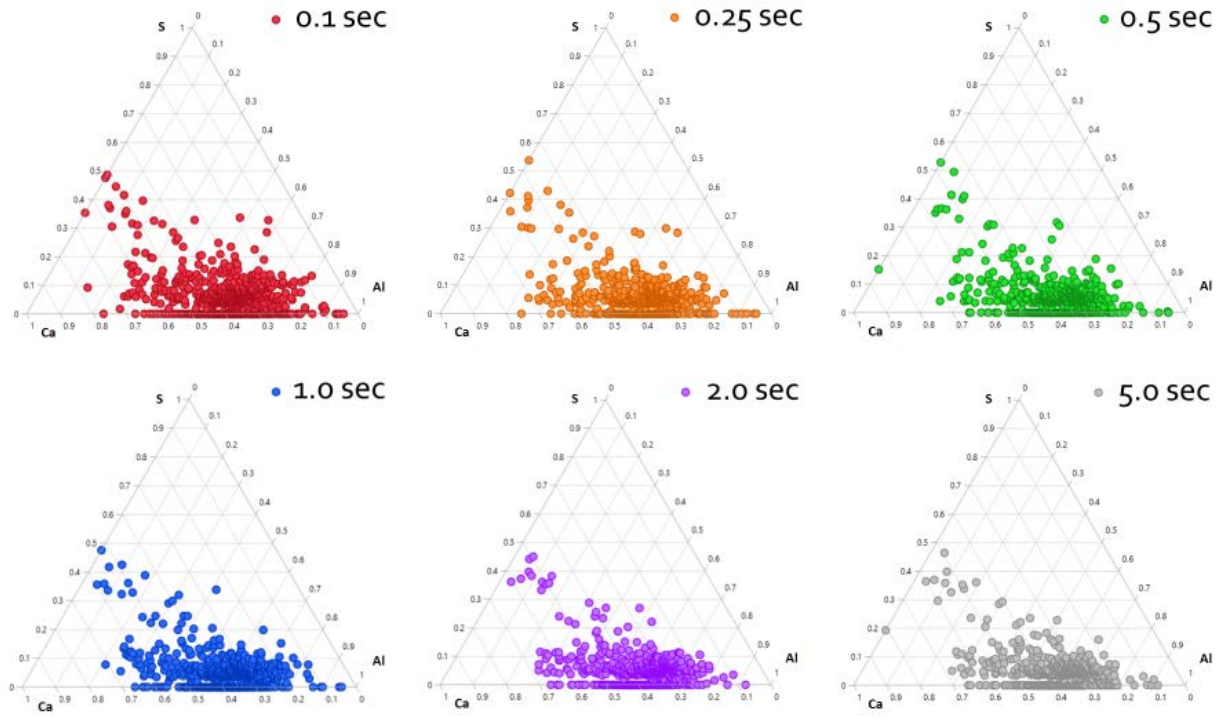

Figure 7 - Ternary Plots Illustrating Various EDS Collection Times

Figure 7 shows Ternary diagrams based on the same experiment shown in Figure 6. Differences in computed inclusion chemistry due to noise would manifest as increased spread when plotted in this format. However, in these diagrams, it does not appear that there is much difference in the spread of the points in spite of the differences in collection time. This shows that, in this example, a shorter collection time did not compromise the spread of measured inclusion compositions.

On the subject of X-ray collection time, we can summarize some general principles:

- General appearance of the spectrum takes shape very quickly.
- For many applications, a short collection time can produce suitable results.
    - The challenge is to determine the minimum collection time that is appropriate for an application.
    - With modern SDD detectors and digital pulse processors, many applications can achieve good results with acquisition times of a fraction of a second.
- For heavily-loaded samples, X-ray collection is a significant component of total analysis time, and speed gains from using shorter collection times can be significant.
    - Reducing collection time from 2 seconds to 1 second, or from 1 second to 0.1 second, can shorten a 1000-inclusion analysis by 15-20 minutes.
- For "clean" samples with relatively few inclusions, the speed to be gained may not be significant.

ACCELERATING VOLTAGE

A fundamental parameter of any analysis performed on an electron microscope is the accelerating voltage, which determines the energy of the electrons that form the electron beam. When the incident beam electrons interact with the specimen, the energy of these electrons is a critical factor in the nature, quantity, and intensity of the various signals that are generated during this interaction, and which are used for forming images and making other measurements.

While beam energy does not have a significant effect on the backscatter coefficient[13] (the relationship between the atomic number of the material and the brightness of the BSE signal), at least above 5kV, there are other significant effects. Of greatest interest for CCSEM are interaction volume, X-ray generation, and beam diameter.

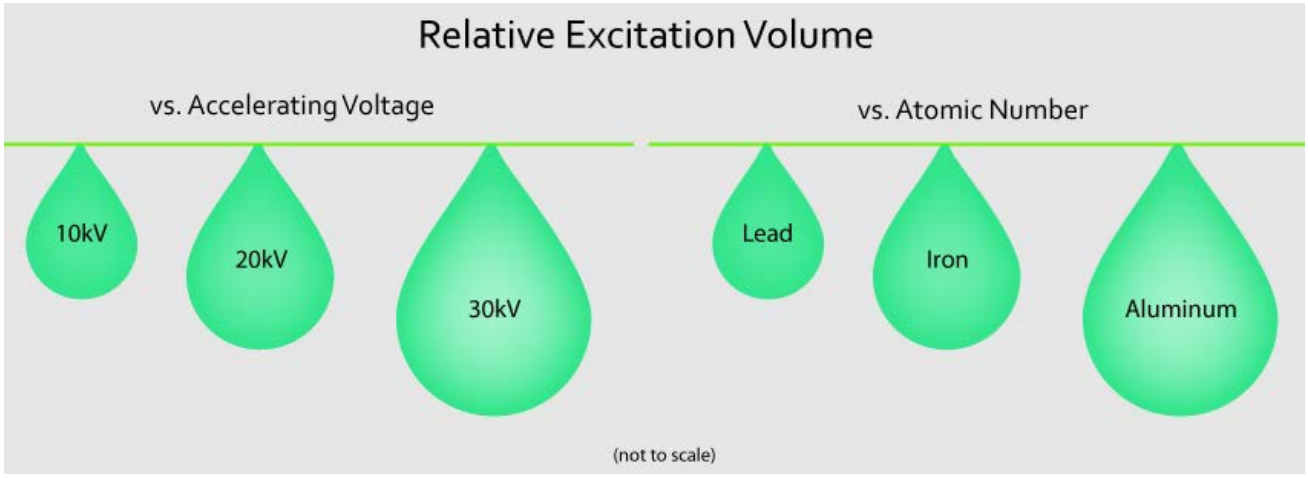

Figure 8 - Comparative Effect of Accelerating Voltage (left) and Atomic Number (right) on Excitation Volume

The interaction volume is the geometric shape under the surface of the specimen in which the incident beam electrons penetrate and spread. It is a roughly teardrop-shaped region of the specimen which forms an envelope in which the beam electrons interact with the atoms of the specimen. It can be generally stated that the depth and width of the teardrop increases with increasing accelerating voltage, and decreases with increasing atomic number (See Figure 8), as described in Equation 4, which is the Kanaya-Okayama equation[14] for beam energies above 5keV:

$$R_{ko} = \frac{0.0276AE^{1.67}}{Z^{0.89}\rho} \quad (4)$$

where A is atomic weight (g/mole); E is incident beam energy (keV); Z is atomic number; and ρ is density in g/cm^3, and R_{ko} represents the maximum depth of interaction. Monte Carlo simulations show that backscattered electrons originate in approximately the topmost 25-40% of this depth, with a lateral spread of radius approximately 40-70% of R_{ko}[15]. But the key takeaway is that in all cases the depth and spread are greater with increasing beam energy.

For this reason, beam-penetration through inclusions and into the steel matrix will influence the BSE signal such that a pixel on an inclusion may appear brighter than it would if the BSE was purely generated within the inclusion. This effect increases with increasing beam energy and decreasing inclusion volume, and can cause diameter measurements to be lower than their true values, and may, in some instances, result in inclusions being missed entirely. This effect is less pronounced when the BSE search/measurement threshold is set inclusive of higher-atomic number inclusions (such as MnS), and more pronounced when the threshold is set to exclude such inclusions[16].

X-ray generation is also affected by the interaction volume, in that a higher accelerating voltage on smaller inclusions will penetrate into the matrix to a greater degree causing a greater number of iron X-rays to be generated and processed by the X-ray detector, although these X-rays are not of interest in characterizing an inclusion.

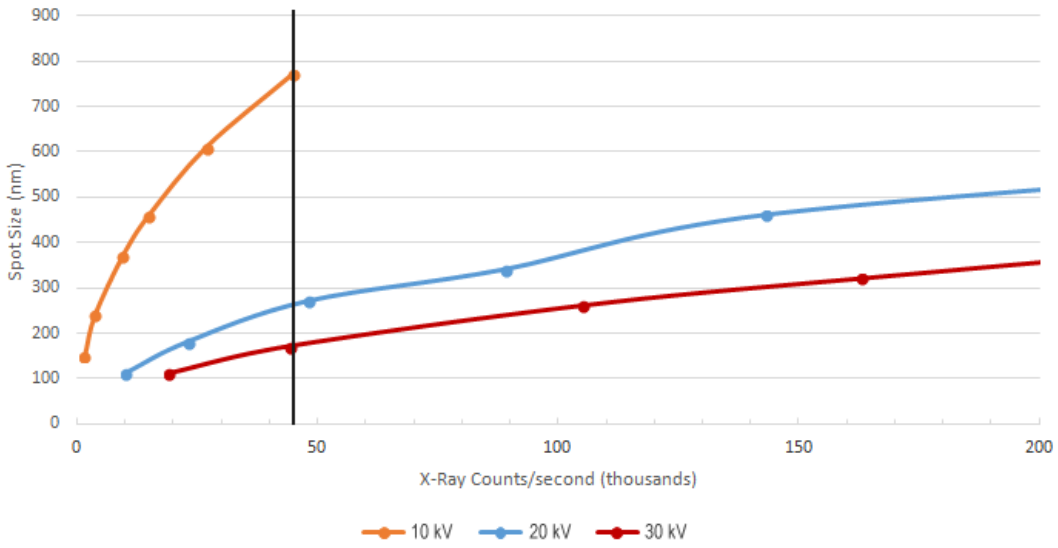

Figure 9 - Spot Size Versus Count Rate for Various Accelerating Voltages. Vertical Line Indicates 45kcps

While lower beam voltage allows less penetration into the steel matrix, it also reduces the incident beam current, and therefore the overall quantity of X-rays produced. For example, on the TESCAN Vega3 SEM used to produce data in this paper, the count rate was plotted versus spot size (beam diameter) for various beam voltages, as computed by the TESCAN In-Flight Beam Tracing™ optical model[17] (see Figure 9). It is noteworthy that to achieve an X-ray count rate of approximately 45 kcps, which is modest for a modern Silicon Drift Detector (SDD), the size of the beam had to be increased from 170nm at 30kV, to 270nm at 20kV, to 770nm at 10kV. While a lower count-rate (and therefore smaller beam diameter) is somewhat offset at lower accelerating voltage due to fewer iron X-rays, it has long been an objective in CCSEM applications to maximize analysis speed while maintaining data quality, and thus it is often preferable to use higher count rates and a higher accelerating voltage will provide better image resolution due to smaller beam diameter. An alternate approach is to use a brighter electron source, which increases the beam current and therefore X-ray count-rate for a given beam diameter, relative to the Tungsten source used to generate the data in this study. For example, a Field Emission source is several orders of magnitude brighter than Tungsten[18] – in other words, it can put the same number of electrons through a much smaller beam diameter relative to the Tungsten source. However, this adds to the cost of the instrumentation and lengthens the time required to achieve break-even on the investment. Another option is a Lanthanum Hexaboride (LaB_6) source, which is less expensive than Field Emission but offers only a comparatively modest brightness improvement over Tungsten[19].

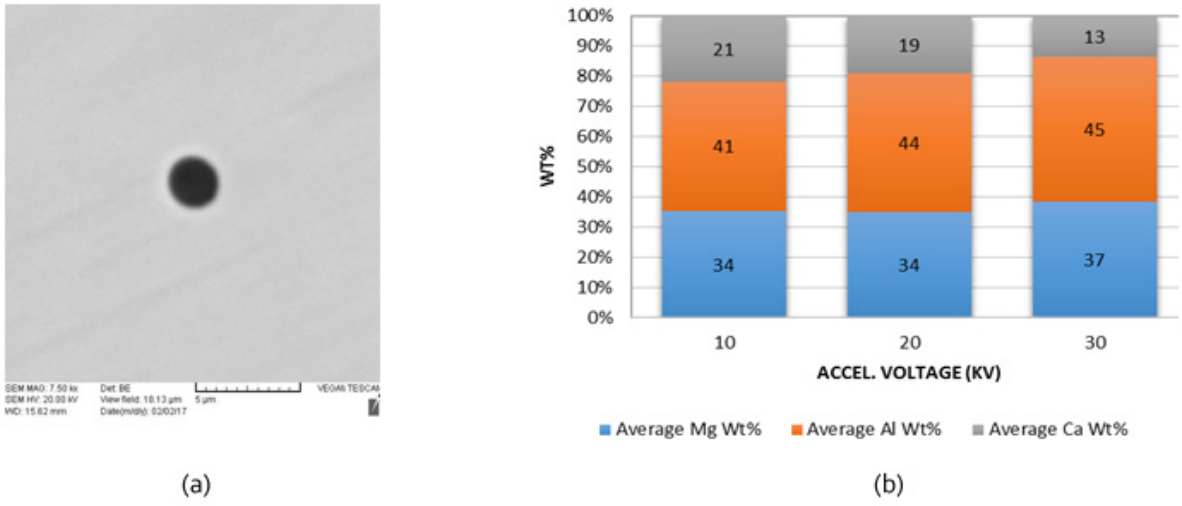

Figure 10 - (a) Backscattered Electron Image of a 2 µm Inclusion; (b) Average Wt% of Ca, Al, and Mg Acquired from the Center of the Inclusions in Figure 10(a)

Another consideration is the distortion of the elemental ratios in inclusions due to absorption effects in the steel matrix, which differs depending on accelerating voltage and may more closely approximate stoichiometric ratios for certain elements at 10kV than at higher accelerating voltages[20]. For example, Figure 10(a) is a backscattered image acquired at 20kV of a 2 µm CaO-Al_2O_3-MgO inclusion. An X-ray spectrum was acquired (2 sec) in a point acquisition from the center of the feature multiple times at three different accelerating voltages. The resultant spectra were quantified using Bruker's Esprit software, and Figure 10(b) provides the average weight percent for each accelerating voltage. The results do show minor differences in the compositions when performing a quantification routine.

In general, lower accelerating voltage results in:

- Less beam penetration
  - Less BSE from steel matrix when beam is hitting small inclusion and edge of inclusion.
    - Potentially improved size measurement accuracy.
    - Better detection probability for small inclusions, especially when thresholding out heavier inclusions like MnS or Ti-containing inclusions, where the atomic number approaches that of Fe more closely.
  - Less X-ray production from matrix when performing X-ray analysis on inclusions.
    - Greater percentage of X-rays processed by detector are from elements of interest.
    - Elemental ratios more closely approach stochiometric for certain elements.
- Lower overall X-ray count rate
  - Longer analysis time.
  - Much larger beam diameter needed for equivalent X-ray count rate.
    - Poorer image resolution.
  - For a given beam diameter, count rate and therefore sample analysis will be slower with lower accelerating voltage.

SUMMARY

Over the last several decades, analysis of inclusions using CCSEM techniques has evolved into a routine practice in the steel industry. However, what has been accomplished thus far represents a small fraction of the potential of this technology. To use this technology effectively in the development of new applications, it is important to understand not only the strengths of the technology but its limitations. Technology such as ASCAT is highly automated, but in the process of making automated inclusion analysis using the SEM routine, the technology has evolved to some extent into a 'black box'. To this end, the purpose of this paper was to provide basic, but critical information related to the effects of various parameters (pixel spacing, X-ray analysis time and accelerating voltage) on CCSEM analysis of inclusions which will help guide researchers in the development of analysis 'recipes' to optimize the use of this technology to its fullest extent.

Future papers will build on the discussions in this paper and focus on the concept that 'less is more' and how the automated inclusion data can be better integrated with the traditional manual SEM analysis as well as analyses using other analytical

techniques to enable an accurate and time efficient assessment of the inclusion population. Achieving an ultra-fast analysis will require use of the latest hardware technologies in tandem with software that processes the inclusion data during the analysis and makes decisions in real time. The incorporation of intelligence into the software will permit each sample to be treated independently based on the numbers and types of inclusions observed during the analysis. In a production environment, the more quickly an accurate assessment of steel cleanliness can be gathered under given operating conditions and practices, the more quickly corrective actions can be taken that improve quality and productivity. Such improvements can contribute to improved steelmaking operations in areas such as enhancing caster refractory life, increasing yield due to a reduced concentration of surface imperfections and improving product properties that enhance the performance of products in service.

ACKNOWLEDGEMENTS

We would like to gratefully acknowledge the assistance of Dr. Scott R. Story of the United States Steel Research Center for providing samples and technical expertise, as well as assisting in the evaluation of data.

REFERENCE

1. T.I. Johansson, T.B. Lund, and P.L.J. Olund, "A Review of Swedish Bearing Steel Manufacturing and Quality Assurance of Steel Products", *Journal of ASTM International*, Vol. 3, No 10, 2006, Paper ID JAI14022
2. United States Steel Research Center Brochure, 1956.
3. R. J. Lee and J. J. McCarthy, "Automatic Image Particle Analysis in Electron Optical Instruments", Eastern *Analytical Symposium*, New York, New York, November 16, 1983.
4. K.F.J. Heinrich, "Electron Probe Microanalysis by Specimen Current Measurement", (*Proc. Fourth International Symposium X-ray Optics and Microanalysis, Orsay*, France, Sept 7-10, 1965), Chapter in *X-ray Optics and Microanalysis*, R. Castaing, P. Deschamps, and J. Philibert, eds., pp. 159-167 (Hermann, Paris, France, 1966)
5. R.J. Lee, J. F. Kelly, "Overview of SEM Based Automated Image Analysis", *Scanning Electron Microscopy*, Vol. 1, SEM Inc., AMF O'Hare, IL, pp 303-310 (1980).
6. P. Kaushik, J. Lehmann, and M. Nadif, "State of the Art of Control of Inclusions, Their Characterization and Future Requirements", *Proceedings of the Richard J. Fruehan Symposium - Physical Chemistry of Sustainable Metals*, Pittsburgh PA June 1-2 2011, pp. 191-212
7. P. Glaws, R.S. Hyde, "On the Effect of Consumable Electrode Remelt Processes on Steel Cleanliness," Bearing Steel Technologies: 10th Volume, Advances in Steel Technologies for Rolling Bearings, STP 1580, John M. Beswick, Ed., pp. 3-15, doi:10.1520/STP158020140098, ASTM International, West Conshohocken, PA, 2015.
8. M. Harris, O. Adaba, S. Lekakh, R. O'Malley, V.L. Richards, "Improved Methodology for Automated SEM/EDS Non-Metallic Inclusion Analysis of Mini-Mill and Foundry Steels," *AISTech 2015 Proceedings*, AIST 2015.
9. "Standard Test Methods for Rating and Classifying Inclusions in Steel Using the Scanning Electron Microscope", *ASTM Designation E2142-08*, ASTM International, West Conshohocken PA, 2015.
10. S. R. Story and F. J. Mannion, "The Use of CCSEM Inclusion Analysis to Improve Steel Quality and Productivity", *Proceedings of the Richard J. Fruehan Symposium*, Pittsburgh PA, 2011.
11. A.J. Schwoeble, A.M. Dalley, B.C. Henderson, and G.S. Casuccio, "Computer-Controlled SEM and Microimaging of Fine Particles", *Journal of Metals*, Vol. 40, No. 8, pp. 11-14, August 1988
12. W. Reuter, in *Proceedings of the 6th International Conference on X-ray Optics and Microanalysis*, G. Shinoda, K. Kohra, and T. Ichinokawa, eds., pp. 121-130 (University of Tokyo Press, Tokyo 1972)
13. J. Goldstein, D. Newbury, D. Joy, C. Lyman, P. Echlin, E. Lifshin, L. Sawyer, and J. Michael, *Scanning Electron Microscopy and X-Ray Microanalysis, Third Edition*, pp. 77-79 (Springer Science + Business Media, New York, 2003)
14. K. Kanaya and S. Okayama, "Penetration and Energy-Loss Theory of Electrons in Solid Targets", *Journal of Physics D: Applied Physics*, Volume 5, Issue 1, pp. 43-58, 1972.
15. D.E. Newbury, and R.L. Myklebust, in *Microbeam Analysis* – 1991, D.G. Howitt, ed, p. 561 (San Francisco Press, San Francisco)

16. D. Tang and P.C. Pistorius, "Optimizing Speed and Quality of Automated Inclusion Analysis", *AISTech Conference Proceedings*, 2015

17. J. Kolosova, T. Hrncir, J. Jiruse, M. Rudolf, and J. Zlamal, "On the Calculation of SEM and FIB Beam Profiles", *Proceedings of the Ninth International Conference on Charged Particle Optics*, Cambridge University Press, Microscopy and Microanalysis, Volume 21, Supplement 4, 2015

18. J. Goldstein, D. Newbury, D. Joy, C. Lyman, P. Echlin, E. Lifshin, L. Sawyer, J. Michael, *Scanning Electron Microscopy and X-Ray Microanalysis, Third Edition*, p. 35 (Springer Science + Business Media, New York, 2003)

19. Ibid.

20. P.C. Pistorius and A. Patadia, "The Steel Matrix Affects Microanalysis of $CaO\text{-}Al_2O_3\text{-}CaS$ Inclusions", *Proceedings of 8th International Conference on Clean Steel*, Budapest, Hungary, 2012